RAA 2015 Vol. **15** No. **1**, 127–144 doi: 10.1088/1674–4527/15/1/012
http://www.raa-journal.org *http://www.iop.org/journals/raa*

Research in Astronomy and Astrophysics

Attitude dynamics and control of spacecraft using geomagnetic Lorentz force

Yehia A. Abdel-Aziz[1,2] and Muhammad Shoaib[2]

[1] National Research Institute of Astronomy and Geophysics (NRIAG), Helwan, Cairo 11721, Egypt; *yehia@nriag.sci.eg*
[2] University of Hail, Department of Mathematics, PO BOX 2440, Kingdom of Saudi Arabia; *safridi@gmail.com*

Received 2014 March 22; accepted 2014 May 12

Abstract Attitude stabilization of a charged rigid spacecraft in Low Earth Orbit using torques due to Lorentz force in pitch and roll directions is considered. A spacecraft that generates an electrostatic charge on its surface in the Earth's magnetic field will be subject to perturbations from the Lorentz force. The Lorentz force acting on an electrostatically charged spacecraft may provide a useful thrust for controlling a spacecraft's orientation. We assume that the spacecraft is moving in the Earth's magnetic field in an elliptical orbit under the effects of gravitational, geomagnetic and Lorentz torques. The magnetic field of the Earth is modeled as a non-tilted dipole. A model incorporating all Lorentz torques as a function of orbital elements has been developed on the basis of electric and magnetic fields. The stability of the spacecraft orientation is investigated both analytically and numerically. The existence and stability of equilibrium positions is investigated for different values of the charge to mass ratio (α^*). Stable orbits are identified for various values of α^*. The main parameters for stabilization of the spacecraft are α^* and the difference between the components of the moment of inertia for the spacecraft.

Key words: space vehicles — atmospheric effects — celestial mechanics — kinematics and dynamics

1 INTRODUCTION

The attitude stabilization of a spacecraft is subject to the perturbation torques which produce turning moments about the center of mass of an orbiting spacecraft. How significant the effect of these torque disturbances is on the spacecraft depends on the configuration of the spacecraft. The perturbation torques may be used to produce a persistent turning moment about the center of mass of the spacecraft.

The present work analyzes the attitude stabilization of a charged spacecraft by taking into account the effects of gravitational torque, geomagnetic torque and Lorentz torque. In the case of an electrostatically charged spacecraft, due to the interaction with space plasma, the Lorentz force must be taken into account as a perturbation on the orbital and attitude motions of the spacecraft.

The nascent concept of a Lorentz spacecraft, which is an electrostatically charged space vehicle, may provide a new approach to the solution of attitude stabilization of a spacecraft moving

around the Earth in low Earth orbit (LEO). Recently, a novel attitude orientation and formation flying concept using electrostatic propulsion has been proposed by Pollock et al. (2011), and Peng & Gao (2012). The charge of the spacecraft is controlled to generate inter-spacecraft Coulomb forces in geostationary orbit. The Lorentz force is a possible means for charging and thus controlling the orbits of the spacecraft without consuming propellant (Hiroshi et al. 2009). Peck (2005) was the first to introduce a control scheme using Lorentz augmented orbits. Orbits of a spacecraft accelerated by the Lorentz force are termed Lorentz-augmented orbits, because the Lorentz force cannot completely replace traditional rocket propulsion. Many authors introduced using the Lorentz force to generate perturbations on the orbital motion and formation flying such as in Vokrouhlicky (1989), Abdel-Aziz (2007a), Streetman & Peck (2007), Hiroshi et al. (2009), Gangestad et al. (2010) and Abdel-Aziz & Khalil (2014).

Abdel-Aziz (2007b) studied the attitude stabilization of a rigid spacecraft moving in a circular orbit due to Lorentz torque in the case of a uniform magnetic field and a spacecraft having a cylindrical shape. Yamakawa et al. (2012) investigated the attitude motion of a charged pendulum spacecraft moving in a circular orbit, having the shape of a dumbbell pendulum due to Lorentz torque. Their analysis of the stability of the equilibrium points only focused on the pitch direction within the equatorial plane. In a recent study, Abdel-Aziz & Shoaib (2014) studied the relation between the magnitude of Lorentz torque and inclination of the orbits for certain equilibrium positions where the spacecraft was considered to be in a circular orbit.

In this paper, we analyze the attitude stabilization of a charged spacecraft moving in the geomagnetic field in LEO. We develop a new model for torque due to the Lorentz force for the general shape of the spacecraft using the Earth's magnetic field, which is modeled as a non-tilted dipole. The total Lorentz force and its torque are developed as a function of orbital elements of the spacecraft. A dynamical model is built to describe the attitude dynamics of the Lorentz spacecraft. Therefore, based on the dynamical model, the required control torque due to Lorentz force for different configurations is developed. The Lorentz acceleration cannot totally replace propellant but can be used to reduce the consumption of propellant. Thus, this paper analyzes the attitude stability of the spacecraft with the Lorentz acceleration and gives the corresponding required specific charge to mass ratio for such attitude orientation. This paper also analyzes the effects of charge to mass ratio on the position and stability of equilibrium positions. We also numerically analyze the behavior of orbits close to the equilibrium positions.

Section 1.1 gives the formulation of a coordinate system to describe the spacecraft. In Section 2, an expression of the Lorentz force and the total torque due to Lorentz force are derived. In Section 3, all possible equilibrium positions are identified, and their stability are analyzed in the pitch and roll directions. Moreover Section 3 gives numerical results to explain the effect of charge to mass ratio on the stability and existence of equilibrium solutions. Conclusions are given in Section 4.

1.1 Formulation of a Coordinate System to Describe the Spacecraft

We assume that the spacecraft is equipped with an electrostatically charged protective shield that has an intrinsic magnetic moment. The attitude orientation of the spacecraft about its center of mass is analyzed under the influence of gravity gradient torque T_{G}, magnetic torque T_{M} and torque T_{L} due to Lorentz force. The torque T_{L} results from the interaction between the geomagnetic field and the charged screen of the electrostatic shield.

We consider the orbital coordinate system $C_{x_{\mathrm{o}}y_{\mathrm{o}}z_{\mathrm{o}}}$ with $C_{x_{\mathrm{o}}}$ tangent to the orbit in the direction of motion, $C_{y_{\mathrm{o}}}$ lies along the normal to the orbital plane and $C_{z_{\mathrm{o}}}$ lies along the radius vector r of the point O_E relative to the center of the Earth. The investigation is carried out assuming there is rotation of the orbital coordinate system relative to the inertial system described by angular velocity Ω. As an inertial coordinate system, the system O_{XYZ} is taken, whose axis $OZ(k)$ is directed along

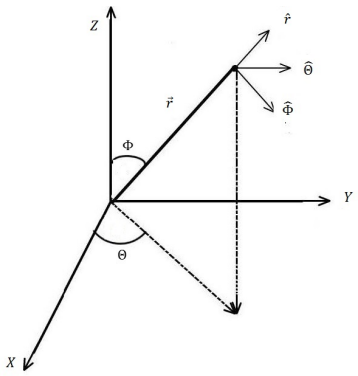

Fig. 1 Spherical coordinates used in the derivation of the equations of motion.

the axis of the Earth's rotation, the axis $OX(i)$ is directed toward the ascending node of the orbit, and the plane coincides with the equatorial plane. Also, we assume that the spacecraft's principal axes of inertia $C_{x_b y_b z_b}$ are rigidly fixed to a spacecraft (i_b, j_b, k_b). The spacecraft's attitude may be described in several ways; in this paper the attitude will be described by the angle of yaw ψ, the angle of pitch θ and the angle of roll φ, between the spacecraft's $C_{x_b y_b z_b}$ and the set of reference axes O_{XYZ}. The three angles are obtained by rotating spacecraft axes from an attitude coinciding with the reference axes to describe attitude in the following way:

– The angle of precession ψ is taken in a plane orthogonal to the Z-axis.

– θ is the rotation angle between the axes Z and z_0.

– ϕ is angle of self-rotation around the Z-axis.

We write the relationship between the reference frames $C_{x_b y_b z_b}$ and $C_{x_o y_o z_0}$ as below (Wertz 1978):

$$A = \begin{pmatrix} \alpha_1 & \alpha_2 & \alpha_3 \\ \beta_1 & \beta_2 & \beta_3 \\ \gamma_1 & \gamma_2 & \gamma_3 \end{pmatrix}, \tag{1}$$

where

$$\begin{aligned} (\alpha_1, \alpha_2, \alpha_3) &= (\cos\psi\cos\phi - \sin\psi\sin\phi\cos\theta, -\cos\psi\sin\phi - \cos\theta\sin\psi\cos\phi, \sin\theta\ \sin\psi), \\ (\beta_1, \beta_2, \beta_3) &= (\sin\psi\cos\varphi + \cos\theta\cos\psi\sin\varphi, -\sin\psi\sin\phi + \cos\theta\cos\psi\cos\phi, -\sin\theta\cos\psi), \\ (\gamma_1, \gamma_2, \gamma_3) &= (\sin\theta\ \sin\phi, \sin\theta\cos\phi, \cos\theta), \end{aligned} \tag{2}$$

and

$$\boldsymbol{\alpha} = \alpha_1 i_b + \alpha_2 j_b + \alpha_3 k_b, \quad \boldsymbol{\beta} = \beta_1 i_b + \beta_2 j_b + \beta_3 k_b, \quad \boldsymbol{\gamma} = \gamma_1 i_b + \gamma_2 j_b + \gamma_3 k_b. \tag{3}$$

2 TOTAL TORQUE DUE TO LORENTZ FORCE

We use spherical coordinates to describe the magnetic and gravitational fields, and the spacecraft trajectory, as shown in Figure 1. The X, Y and Z axes form a set of inertial Cartesian coordinates. The Earth is assumed to rotate about the Z-axis. The magnetic dipole is not tilted and therefore is axisymmetric. The spherical coordinates consist of radius r, colatitude angle Φ and azimuth from the X direction Θ (see Fig. 1). The magnetic field is expressed as

$$\boldsymbol{B} = \frac{B_0}{r^3}\left[2\cos\Phi\ \hat{r} + \sin\Phi\ \hat{\Phi} + \mathbf{0}\hat{\Theta}\right], \tag{4}$$

where B_0 is the strength of the magnetic field in Wb m. The acceleration in inertial coordinates is given by

$$\boldsymbol{a}=\frac{\boldsymbol{F}}{m}=-\frac{\mu}{r^3}\boldsymbol{r}+\frac{q}{m}(\boldsymbol{E}+\boldsymbol{V}_{\rm rel}\times\boldsymbol{B}), \tag{5}$$

where $\frac{q}{m}$ is the charge-to-mass ratio of the spacecraft and $\boldsymbol{V}_{\rm rel}$ is the velocity of the spacecraft relative to the magnetic field of the Earth. The total Lorentz force (per unit mass) can be written as

$$\begin{aligned}\boldsymbol{F}_{\rm L} &= \frac{q}{m}\left[\boldsymbol{E}+\boldsymbol{V}_{\rm rel}\times\boldsymbol{B}\right]=\frac{q}{m}\boldsymbol{E}+\frac{q}{m}(\boldsymbol{V}_{\rm rel}\times\boldsymbol{B})\\ &= \boldsymbol{F}_{\rm elec}+\boldsymbol{F}_{\rm mag},\end{aligned} \tag{6}$$

where $\boldsymbol{F}_{\rm mag}$ is the Lorentz force experienced by a point in the magnetic field and $F_{\rm elec}$ is the Lorentz force experienced by an electric dipole moment in the presence of an electric field,

$$\boldsymbol{F}_{\rm elec}=\frac{q}{m}\boldsymbol{E}\,. \tag{7}$$

Now starting with $\boldsymbol{F}_{\rm mag}$ using Maxwell (1861), we can write

$$\boldsymbol{F}_{\rm mag}=\frac{q}{m}(\boldsymbol{V}_{\rm rel}\times\boldsymbol{B})\,,\qquad \boldsymbol{V}_{\rm rel}=\boldsymbol{V}-\boldsymbol{\omega_e}\times\boldsymbol{r}\,, \tag{8}$$

where $\boldsymbol{V}$ is the inertial velocity of the spacecraft and ω_e is the angular velocity vector of the Earth. According to Gangestad et al. (2010), we use

$$\boldsymbol{V}=\dot r\,\hat r+r\dot\Phi\hat\Phi+r\,\dot\Theta\sin\Phi\,\hat\Theta\,,$$

and

$$\boldsymbol{r}\;=r\,\hat r\,,\quad \boldsymbol{\omega_e}=\omega_e\,\hat z\,,\quad \hat z\;=\cos\Phi\hat r+\sin\Phi\;\hat\Phi\,. \tag{9}$$

Therefore the acceleration in inertial coordinates is given by

$$\boldsymbol{F}_{\rm mag}=\frac{qB_0}{m\,r^2}\left[\begin{array}{c}-\left(\dot\Theta-\omega_e\right)\left(\sin^2\Phi\,\hat r+\sin(2\Phi)\hat\Phi\right)\\ +\left(\frac{\dot r}{r}\sin\Phi-2\dot\Phi\;\cos\Phi\right)\hat\Theta\end{array}\right]. \tag{10}$$

In the case of torque we need the perturbing force $\boldsymbol{F}_{\rm L}$ decomposed into the radial, transverse and normal directions. The unit vector $\hat n$ normal to the orbit is collinear with the angular momentum unit vector $\hat h$.

$$\hat n=\hat h=(\boldsymbol{r}\times\boldsymbol{V})\,/\sqrt{\mu p}=r^2/\sqrt{\mu p}(-\dot\Theta\sin\Phi\hat\Phi+\dot\Phi\hat\Theta), \tag{11}$$

where $p=a(1-e^2)$, μ is the Earth's gravitational parameter, a is the semimajor axis, e is the eccentricity of the spacecraft's orbit, and the transverse unit vector $\hat t$ can be calculated from the right-hand rule, $\hat t=\hat n\times\hat r$. Decomposition of the Lorentz force experienced by the geomagnetic field into the radial, transverse and normal components $(R_{\rm mag},T_{\rm mag},\;N_{\rm mag})$ respectively yields,

$$R_{\rm mag}=\boldsymbol{F}_{\rm mag}\cdot\hat r\;=\frac{q}{m}\frac{B_0}{r^2}\left[\omega_e-\dot\Theta\right]\sin^2\Phi, \tag{12}$$

$$T_{\rm mag}=\boldsymbol{F}_{\rm mag}\cdot\hat t\;=\frac{q}{m}\frac{B_0}{\sqrt{\mu p}}\left[\begin{array}{c}\frac{\dot r}{r}\dot\Theta\sin^2\Phi\\ -2\omega_e\,\dot\Phi\cos\Phi\sin\Phi\end{array}\right], \tag{13}$$

$$N_{\rm mag}=\boldsymbol{F}_{\rm mag}\cdot\hat n\;=\frac{q}{m}\frac{B_0}{\sqrt{\mu p}}\left[\begin{array}{c}2\dot\Theta(\omega_e-\dot\Theta)\sin^2\Phi\cos\Phi\\ +\frac{\dot r}{r}\dot\Theta\sin\Phi-2\dot\Phi^2\;\cos\Phi\end{array}\right]. \tag{14}$$

The relationship between the spherical coordinates and the orbital elements is required to derive the components of Lorentz force experienced by the magnetic component as a function of orbital elements.

$$r = p/\left(1 + e\ \cos f\right)\,, \qquad \dot{r} = e\sqrt{\mu/p}\sin f\,, \tag{15}$$

$$\cos\Phi = \sin i \sin\left(\omega^* + f\right)\,, \qquad \sin\Phi = \sqrt{1 - \sin^2 i \sin^2\left(\omega^* + f\right)}, \tag{16}$$

$$\dot{\Phi} = -\sqrt{\mu/p^3}\frac{\sin i \cos\left(\omega^* + f\right)}{\sqrt{1 - \sin^2 i \cos^2\left(\omega^* + f\right)}}\left(1 + e\ \cos f\right)^2\,, \tag{17}$$

$$\dot{\Theta} = \sqrt{\mu/p^3}\frac{\cos i}{1 - \sin^2 i \sin^2\left(\omega^* + f\right)}\left(1 + e\ \cos f\right)^2\,, \tag{18}$$

where i, ω^* and f are the inclination of the orbit with respect to the equator, argument of the perigee and the true anomaly in the spacecraft's orbit respectively. Therefore, rewriting the components of the magnetic part of the Lorentz force as a function of orbital elements, we obtain

$$R_{\text{mag}} = \frac{q}{m}\frac{B_0}{r^2}\begin{bmatrix} \omega_e(1 - \sin^2 i \sin^2\left(\omega^* + f\right)) \\ -\sqrt{\mu/p^3}\cos i\ \left(1 + e\ \cos f\right)^2 \end{bmatrix}, \tag{19}$$

$$T_{\text{mag}} = \frac{q}{m}\frac{B_0}{\sqrt{\mu p}}\begin{bmatrix} \frac{\dot{r}}{r}\sqrt{\mu/p^3}\cos i\ \left(1 + e\ \cos f\right)^2 + 2\omega_e\ \sqrt{\mu/p^3}\sin^2 i \sin\left(\omega^* + f\right) \\ \times \cos\left(\omega^* + f\right)\left(1 + e\ \cos f\right)^2 \end{bmatrix}, \tag{20}$$

$$N_{\text{mag}} = \frac{q}{m}\frac{B_0}{\sqrt{\mu p}} \times \tag{21}$$
$$\begin{Bmatrix} 2\left[\omega_e(1 - \sin^2 i \sin^2\left(\omega^* + f\right)) - \sqrt{\mu/p^3}\cos i\ \left(1 + e\ \cos f\right)^2\right] \\ \sqrt{\mu/p^3}\cos i\ \left(1 + e\ \cos f\right)^2\ + \frac{\dot{r}}{r}\sqrt{\mu/p^3}\frac{\cos i}{\sqrt{1-\sin^2 i \sin^2(\omega^*+f)}} \\ \times \left(1 + e\ \cos f\right)^2 - 2\frac{\mu}{p^3}\frac{\sin^3 i \cos^2(\omega^*+f)\sin(\omega^*+f)}{1-\sin^2 i \cos^2(\omega^*+f)}\left(1 + e\ \cos f\right)^4 \end{Bmatrix}.$$

Now we develop the Lorentz force experienced by electric field F_{elec}. According to Ulaby (2005) and Heilmann et al. (2012) we can write the electric force as follows.

$$\boldsymbol{F}_{\text{elec}} = -\nabla \boldsymbol{V}_{\text{elec}} = \left(\frac{\partial\, V_{\text{elec}}}{\partial r}\hat{r} + \frac{1}{r}\frac{\partial\, V_{\text{elec}}}{\partial \Phi}\hat{\Phi} + \frac{1}{r\sin\Theta}\frac{\partial\, V_{\text{elec}}}{\partial \Theta}\hat{\Theta}\right), \tag{22}$$

where $\boldsymbol{V}_{\text{elec}}$ is the electric potential,

$$V_{\text{elec}} = \frac{\boldsymbol{P}\cdot\hat{r}}{4\pi\ \epsilon_{\text{o}} r^2}\,. \tag{23}$$

$\boldsymbol{P} = q\boldsymbol{d}$ is called the electric dipole moment, $\boldsymbol{d}$ is the distance vector from charge $-q$ to charge $+q$ and $\epsilon_{\text{o}} = 8.85 \times 10^{-12}\ \text{C}^2/(N - m^2) \equiv \text{V}^{-1}\text{m}^{-1}$ is the permittivity of free space. Then the final form of the Lorentz force experienced by an electric dipole moment in the presence of an electric field is

$$\boldsymbol{F}_{\text{elec}} = \frac{qd}{4\pi\ \epsilon_{\text{o}} r^3}\left(2\cos\Phi\ \hat{r} + \sin\Phi\ \hat{\Phi} + \mathbf{0}\ \hat{\Theta}\right)\,. \tag{24}$$

Similarly as we did for the magnetic force, we can write the radial, transverse and normal components $(R_{\text{elec}}, T_{\text{elec}},\ N_{\text{elec}})$ of the electric force,

$$R_{\text{elec}} = -\frac{q}{m}\frac{d}{4\pi\ \epsilon_{\text{o}} r^3}\left(\omega_e - \dot{\Theta}\right)\sin^2\Phi. \tag{25}$$

$$T_{\text{elec}} = \boldsymbol{F}_{\text{elec}} \cdot \hat{t} \; = \frac{q}{m} \frac{d}{4\pi \; \epsilon_{\text{o}} r^3} \frac{r^3}{\sqrt{\mu \; a \left(1 - e^2\right)}} \left(\omega_e - \dot{\Theta}\right) \; \dot{\Phi} \sin \Phi \; \cos \Phi. \tag{26}$$

$$\begin{aligned} N_{\text{elec}} \; &= \; \boldsymbol{F}_{\text{elec}} \cdot \hat{n} \\ &= \; \frac{q}{m} \frac{d}{4\pi \; \epsilon_{\text{o}} r^3} \frac{r^2}{\sqrt{\mu \; a \left(1 - e^2\right)}} \left(\omega_e - \dot{\Theta}\right) \; \dot{\Theta} \; \sin^2 \Phi \; \cos \Phi. \end{aligned} \tag{27}$$

Similarly, we can write the components of the Lorentz force experienced by an electric field as a function of orbital elements as follows.

$$R_{\text{elec}} = -\frac{q}{m} \frac{d}{4\pi \; \epsilon_{\text{o}} r^3} \left[\begin{array}{c} \omega_e \left(1 - \sin^2 i \sin^2 \left(\omega^* + f\right)\right) - \\ \sqrt{\mu / a^3 \left(1 - e^2\right)^3} \; \cos i \; \left(1 + e \; \cos f\right)^2 \end{array} \right]. \tag{28}$$

$$\begin{aligned} T_{\text{elec}} \; = \; & \frac{q}{m} \frac{d}{4\pi \; \epsilon_{\text{o}} r^2} \times \\ & \left[\omega_e - \sqrt{\mu / a^3 \left(1 - e^2\right)^3} \frac{\cos i \; \left(1 + e \; \cos f\right)^2}{1 - \sin^2 i \sin^2 \left(\omega^* + f\right)} \right] \sin^2 i \cos \left(\omega^* + f\right) \sin \left(\omega^* + f\right). \end{aligned} \tag{29}$$

$$\begin{aligned} N_{\text{elec}} \; = \; & \frac{q}{m} \frac{d}{4\pi \; \epsilon_{\text{o}} r^3} \times \\ & \left[\omega_e - \sqrt{\mu / a^3 \left(1 - e^2\right)^3} \frac{\cos i \; \left(1 + e \; \cos f\right)^2}{1 - \sin^2 i \sin^2 \left(\omega^* + f\right)} \right] \sin i \; \cos i \sin \left(\omega^* + f\right) \; . \end{aligned} \tag{30}$$

Here, we assume that the spacecraft is equipped with a charged surface (screen) of area S with electric charge $q = \int_S \sigma \, dS$ distributed over the surface with density σ. Therefore, as in Tikhonov et al. (2011), we can write the torque of these forces relative to the spacecraft's center of mass as follows.

$$\boldsymbol{T}_{\text{L}} = \boldsymbol{T}_{\text{mag}} + \boldsymbol{T}_{\text{elec}} = \int_S \sigma \boldsymbol{\rho} \times (\boldsymbol{E} + \boldsymbol{V} \times \boldsymbol{B}) dS, \tag{31}$$

where $\boldsymbol{\rho}$ is the radius vector of the screen's element dS relative to the spacecraft's center of mass and $\boldsymbol{V}$ is the velocity of the element dS relative to the geomagnetic field. Finally, the torque due to Lorentz force can be written as follows:

$$\boldsymbol{T}_{\text{mag}} = \boldsymbol{\rho}_0 \times A^{\text{T}} \left(R_{\text{mag}}, T_{\text{mag}}, \; N_{\text{mag}}\right)^{\text{T}}, \quad \boldsymbol{T}_{\text{elec}} = \boldsymbol{\rho}_0 \times A^{\text{T}} \left(R_{\text{elec}}, T_{\text{elec}}, \; N_{\text{elec}}\right)^{\text{T}}, \tag{32}$$

$$\boldsymbol{\rho}_0 = x_0 i_b + y_0 j_b + z_0 k_b = q^{-1} \int_S \sigma \, \boldsymbol{\rho} \, dS \, , \tag{33}$$

where $\boldsymbol{\rho}_0$ is the radius vector of the center of a charged spacecraft relative to its center of mass and A^{T} is the transpose of the matrix A.

2.1 Geomagnetic Field Model and Its Torque

In this paper, we are using a non-tilted dipole for the geomagnetic field. Let a dipole magnetic field be $\boldsymbol{B} = (B_1, B_2, B_3)$, and the magnetic moment of the spacecraft be $\boldsymbol{M} = (m_1, m_2, m_3)$. Therefore the torque due to the geomagnetic field is

$$\boldsymbol{T}_{\text{M}} = \boldsymbol{M} \times \boldsymbol{B} \, . \tag{34}$$

As in Wertz (1978) we can write geomagnetic field and the total magnetic moment of the orbital system directed to the tangent of the orbital plane, normal to the orbit and in the direction of the radius respectively as below:

$$B_1 = \frac{B_0}{2r^3}\sin\theta'_m\left[3\cos(2f-\alpha_m)+\cos\alpha_m\right], \quad B_2 = -\frac{B_0}{2r^3}\cos\theta'_m\,, \tag{35}$$

$$B_3 = \frac{B_0}{2r^3}\sin\theta'_m\left[3\sin(2f-\alpha_m)+\sin\alpha_m\right]. \tag{36}$$

$$m_1 = m\,\sin\theta'_m\cos\alpha_m\,\beta_1,\;\; m_2 = m\,\sin\theta'_m\sin\alpha_m\,\beta_2,\;\; m_3 = m\,\cos\theta'_m\,\beta_3, \tag{37}$$

where $B_0 = -8\times10^{-15}$, $\theta'_m = 168.6^\circ$ is the co-elevation of the dipole, $\alpha_m = 109.3^\circ$ is the east longitude of the dipole, f is the true anomaly measured from the ascending node and m is the magnitude of the total magnetic moment.

3 EQUATIONS DESCRIBING THE ATTITUDE MOTION

The nonlinear differential equation that comes from the Euler and Poisson equations is used to describe the attitude orientation of the spacecraft.

$$\dot{\boldsymbol{\omega}}I + \boldsymbol{\omega}\times\boldsymbol{\omega}I = \boldsymbol{T}_{\rm G} + \boldsymbol{T}_{\rm M} + \boldsymbol{T}_{\rm L}, \tag{38}$$

$$\dot{\boldsymbol{\alpha}} + \boldsymbol{\alpha}\times\boldsymbol{\omega} = -\Omega\boldsymbol{\gamma}, \quad \dot{\boldsymbol{\beta}} + \boldsymbol{\beta}\times\boldsymbol{\omega} = 0, \quad \dot{\boldsymbol{\gamma}} + \boldsymbol{\gamma}\times\boldsymbol{\omega} = \Omega\boldsymbol{\alpha}\,, \tag{39}$$

where $\boldsymbol{T}_{\rm G} = 3\Omega^2\boldsymbol{\gamma}\times\boldsymbol{\gamma}I$ is the well known formula for the gravity gradient torque,

$I = \mathrm{diag}(A,B,C)$ is the inertia matrix of the spacecraft, Ω is the orbital angular velocity and $\boldsymbol{\omega}$ is the angular velocity vector of the spacecraft. According to Wertz (1978) the angular velocity of the spacecraft in the inertial reference frame is $\boldsymbol{\omega} = (p,q,r)$, where

$$p = \dot{\psi}\sin\theta\sin\phi + \dot{\theta}\,\cos\phi, \quad q = \dot{\psi}\sin\theta\cos\phi - \dot{\theta}\,\sin\phi, \quad r = \dot{\psi}\cos\theta + \dot{\phi}\,. \tag{40}$$

3.1 Equations of Motion in the Pitch Direction

In this section, the attitude motion of the spacecraft in the pitch direction is considered, i.e. $\psi = \phi = 0,\ \theta \neq 0$. Applying this condition in Equation (38), we can derive the second order differential equation of the motion in the pitch direction.

$$\begin{aligned} A\frac{d^2\theta}{dt^2} &= (C-B)(3\Omega^2-1)\sin\theta\cos\theta + z_0\sin\theta(\,N_{\rm mag} - kT_{\rm mag}) \\ &\quad + z_0\cos\theta(kN_{\rm mag} - T_{\rm mag}) + z_0\sin\theta(\,N_{\rm elec} - kT_{\rm elec}) \\ &\quad + z_0\cos\theta(kN_{\rm elec} - T_{\rm elec}) + m_2B_3\sin\theta + m_3B_2\cos\theta\,. \end{aligned} \tag{41}$$

Let $y_0 = k\,z_0$, where k is an arbitrary number.

$$\begin{aligned} A\ddot{\theta} &= \left(3\Omega^2-1\right)(C-B)\sin\theta\cos\theta + z_0\sin\theta(N_{\rm mag} - kT_{\rm mag}) \\ &\quad + z_0\cos\theta(kN_{\rm mag} - T_{\rm mag}) + z_0\sin\theta(N_{\rm elec} - kT_{\rm elec}) \\ &\quad + z_0\cos\theta(kN_{\rm elec} - T_{\rm elec}) + B_2m_3\sin\theta + B_3m_2\cos\theta \\ &= g(k, z_0, \alpha^* = q/m, \theta)\,, \end{aligned} \tag{42}$$

where $T_{\rm mag}$, $N_{\rm mag}$, $T_{\rm elec}$ and $N_{\rm elec}$ are defined in Equations (20), (21), (29) and (30) respectively.

A comparison showing the oscillations of $\dot{\theta}$ is given in Figures 2 and 3. It is obvious from the first two figures that the most significant amount of torque is coming from the magnetic part of the Lorentz torque which is of the order 10^{-3}. The effect from the electric part of the Lorentz torque is

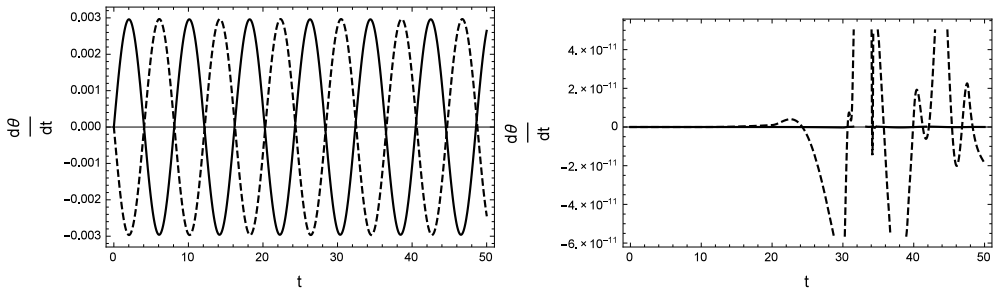

Fig. 2 Oscillation in $\frac{d\theta}{dt}$ due to the (*left*) magnetic part of the Lorentz torque and (*right*) due to the electric part of the Lorentz torque. The dashed line corresponds to $\alpha^* = -0.1$ and the continuous line corresponds to $\alpha^* = 0.1$.

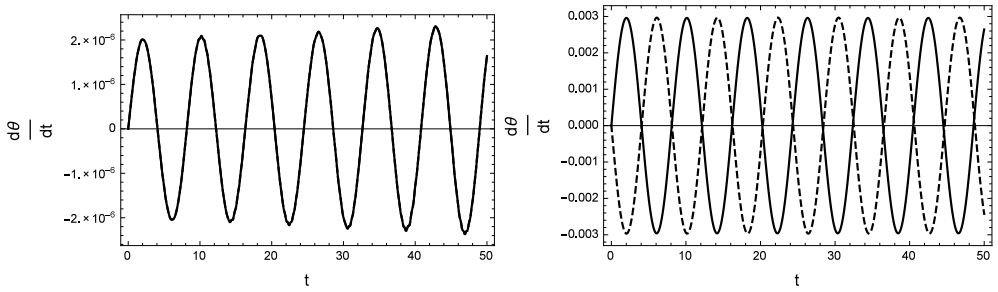

Fig. 3 Oscillation in $\frac{d\theta}{dt}$ due to (*left*) geomagnetic torque and (*right*) torque due to total Lorentz force and the geomagnetic field. The dashed line corresponds to $\alpha^* = -0.1$ and the continuous line corresponds to $\alpha^* = 0.1$. On the left, both the lines for $\alpha^* = \pm 0.1$ overlap.

of the order 10^{-11} which is very small. The contribution from geomagnetic torque is of the order 10^{-6}. The oscillation in $\dot{\theta}$ due to total torque is of the order 10^{-3}, as shown in Figure 3 (right). As the contribution from the electric part of Lorentz force and geomagnetic field is very small compared to the magnetic part of Lorentz force, it does not show up in Figure 3 (left). These figures are drawn for fixed values of $B = 0.7$, $C = 0.1$ and $\alpha^* = \pm 1$.

3.2 Derivation of Equilibrium Solutions in the Pitch Direction and Their Linear Stability Analysis

In this section, the existence and stability of the equilibrium position in the pitch direction of a spacecraft with a general shape under the influence of gravitational torque, Lorentz torque and geomagnetic torque will be discussed. The stability of the equilibrium solutions derived will be discussed both analytically and numerically. To find the equilibrium solutions, set the right hand side of Equation (42) equal to zero which reduces to the following equation for $B = 0.7,\ C = 0.1,\ a = 6900\ \text{km},\ i = 51^\circ,\ e = 0.001$ and $f = 60^\circ$.

$$\begin{aligned} g(k, z_0, \alpha^*, \theta) \ = \ & (2.34 \times 10^{-7} + (0.015 + 0.008k) z_0 \alpha^*) \cos\theta \\ & + (1.56 \times 10^{-6} + (0.008 + 0.015k) z_0 \alpha^*) \sin\theta + 0.3 \sin 2\theta = 0. \end{aligned} \tag{43}$$

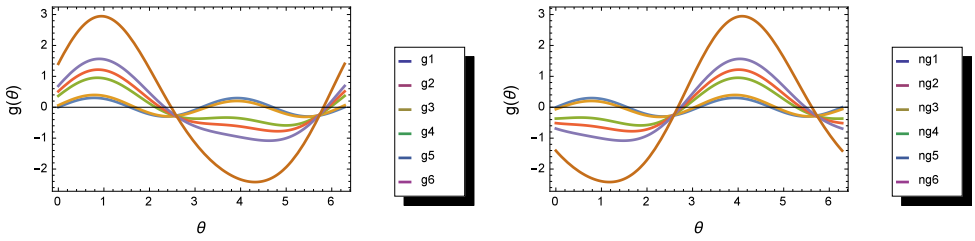

Fig. 4 Progression of equilibrium solutions when (*left*) g1: $(\alpha^*, k) = (0.1, 1)$, g2: $(\alpha^*, k) = (2, 2)$, g3: $(\alpha^*, k) = (5, 7)$, g4: $(\alpha^*, k) = (7, 7)$, g5: $(\alpha^*, k) = (7, 10)$, g6: $(\alpha^*, k) = (10, 15)$ and (*right*) when ng1: $(\alpha^*, k) = (-0.1, 1)$, ng2: $(\alpha^*, k) = (-2, 2)$, ng3: $(\alpha^*, k) = (-5, 7)$, ng4: $(\alpha^*, k) = (-7, 7)$, ng5: $(\alpha^*, k) = (-7, 10)$, ng6: $(\alpha^*, k) = (-10, 15)$.

It is not possible to solve Equation (43) in a closed form as $\theta = f(k, z_0, \alpha^*)$, therefore numerical techniques are used to identify all the roots of Equation (43). As Equation (42) is derived by taking $y = kz_0$, without loss of generality we take $z_0 = 1$. For $0 < \alpha^* < 1$ and $0 < k < 1$, we have five equilibrium solutions at $\theta \approx \frac{n\pi}{2}, n = 0, 1, 2, 3, 4$ when $\theta \in [0, 2\pi]$. As $g(k, \alpha^*, \theta)$ is a periodic function with period 2π, it is sufficient to investigate the equilibrium solutions from 0 to 2π. For $0 < \alpha^* < 1$ and $k \leq 100$ there are five equilibrium solutions which reduce to three or two when $k > 100$. For sufficiently high values of α^*, the number of equilibrium solutions can be reduced to three for even smaller values of α^*. To see the progression of roots from five to three, see Figure 4 where $g(k, \alpha^*, \theta)$ is plotted for various fixed values of k and α^*. To completely describe the progression of the number of equilibrium positions in $[0, 2\pi]$ from five to two, a 3D implicit plot of $g(k, \alpha^*, \theta) = 0$ is given in Figure 5. It can easily be seen that for high enough values of α^* and k, the number of equilibrium points reduces to two. It is also obvious from these figures that the equilibrium positions do not always remain at $\theta \approx \frac{n\pi}{2}, n = 0, 1, 2....$ By comparing Figure 4 left and Figure 4 right it is evident that the equilibrium positions are not the same for positively and negatively charged spacecrafts. It remains to be seen if this or the other parameters such as α^* or k affect the stability of the equilibrium points.

To discuss the linear stability of the equilibrium points identified above, we use the standard procedure of linearization and convert Equation (42) to a system of two first order equations. We then find the eigenvalues of the Jacobian matrix from the equation given below.

$$\lambda^2 - \frac{\partial g(k, z_0, \alpha^*, \theta)}{\partial \theta} = 0\,, \tag{44}$$

where

$$\begin{aligned} \frac{\partial g(k, z_0, \alpha^*, \theta)}{\partial \theta} \;=\; & A^{-1}(\cos\theta\big(1.56 \times 10^{-6} + 10^{-3}(8{+}15k)z_0\alpha^*\big) \\ & +(B - C)\cos(2\theta) - \sin\theta(2.34 \times 10^{-7} + 10^{-3}(15{+}8k)z_0\alpha^*))\,. \end{aligned} \tag{45}$$

It is clear from Equation (44) that there are only two types of eigenvalues possible. If $g_\theta(k, z_0, \alpha^*, \theta) > 0$ there will be two eigenvalues, one of which is negative and one positive. A positive eigenvalue will always imply instability. If $g_\theta(k, z_0, \alpha^*, \theta) < 0$ the eigenvalues obtained will be imaginary with a zero real part which means the equilibrium point in question will be spectrally stable. Initially, we will investigate the equilibrium points obtained above for $A = 1, B = 0.7, C = 0.1$

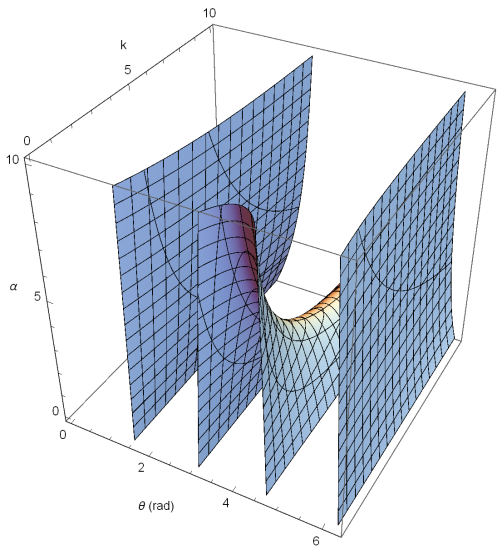

Fig. 5 Implicit plot of $g(k, \alpha^*, \theta) = 0$ when $z_0 = 1$.

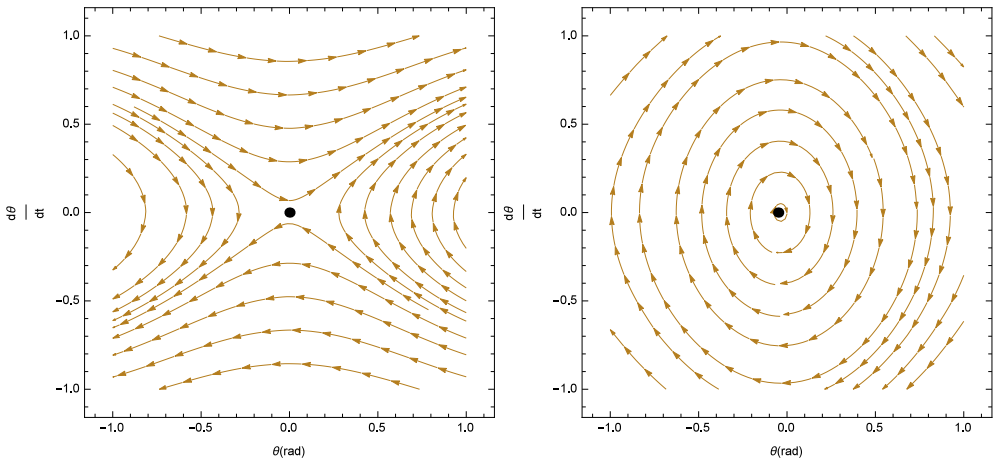

Fig. 6 Trajectory in the $\theta - \frac{d\theta}{dt}$ phase plane when (*left*) $\alpha^* = 0.01, k = 1, z_0 = 1, A = 1, B = 0.7$ and $C = 0.1$, (*right*) $\alpha^* = -1, k = 100, z_0 = 1, A = 1, B = 0.7$ and $C = 0.1$.

and $z_0 = 1$.

$$\frac{\partial g(k, \alpha^*, \theta)}{\partial \theta} = g_\theta = \cos\theta(1.56 \times 10^{-6} + 10^{-3}(8 + 15k)\alpha^*) + 0.6\cos(2\theta) - \sin\theta(2.34 \times 10^{-7}) + 10^{-3}\sin\theta(15 + 8k)\alpha^*. \quad (46)$$

The values of $g_\theta|_{\theta=0}$ and $g_\theta|_{\theta=2\pi}$ remain positive for all positive values of k and α^* which implies that the equilibrium positions at $\theta = 0$ and $\theta = 2\pi$ are unstable. The value of $g_\theta|_{\theta=\pi/2}$ is negative for all positive values of k and α^* which implies that the equilibrium position at $\theta = \pi/2$ will be stable. By similar argument, the equilibrium position at $\theta = \pi$ will be stable if α^* satisfies

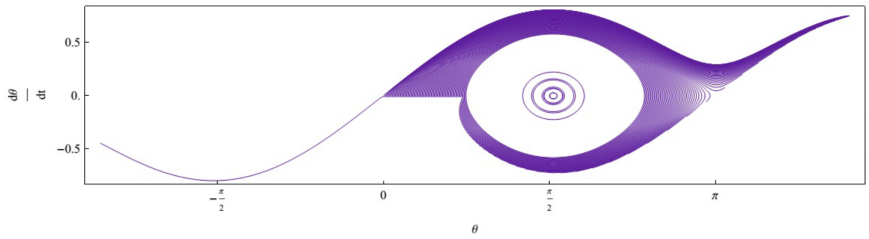

Fig. 7 A set of orbits with initial positions close to $(\theta, \dot{\theta}) \to (0+, 0+)$ in the $\theta - \frac{d\theta}{dt}$ phase plane when $\alpha^* = 0.01, k = 1, z_0 = 1, A = 1, B = 0.7$ and $C = 0.1$.

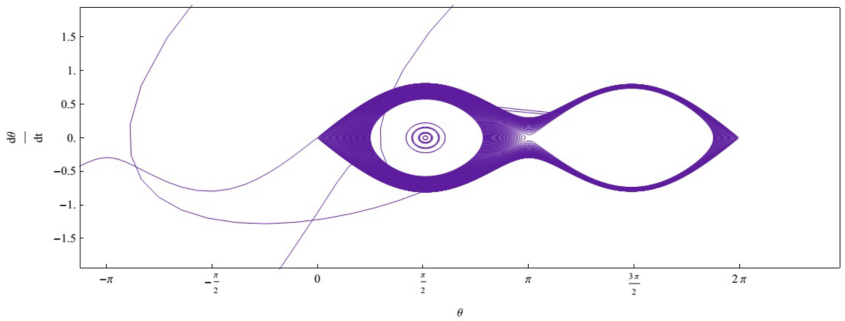

Fig. 8 Same orbits as in Fig. 7 but integrated for a much longer time.

the following inequality.

$$\alpha^* > \frac{0.6}{0.008 + 0.015k} = \alpha_1^* .$$

This also means that $\theta = \pi$ will always be unstable if the spacecraft is negatively charged as the right hand side of the above inequality is always positive. To check the stability of the remaining four equilibrium positions when $\alpha^* < 0$, let $\alpha^* = -\alpha_p$ such that $\alpha_p > 0$. It can easily be shown that the equilibrium position at $\theta = 0$ and $\theta = 2\pi$ will be stable if $\alpha_p < \alpha_1^*$. For example, when $k = 1$, α_p must be smaller than 26.09. Similarly, for the equilibrium position at $\theta = \pi/2$ to be stable for a negatively charged spacecraft, α_p must satisfy the following inequality.

$$\alpha_p < \frac{0.6}{0.008k + 0.015} .$$

It can be safely concluded from this discussion that the sign and amount of charge on the spacecraft play a significant role in the stability of the equilibrium positions. A typical trajectory in the $\theta - \frac{d\theta}{dt}$ phase plane around $\theta = 0$ is given in Figure 6 for $\alpha^* = 0.01, -1$, $k = 1, 100$, $z_0 = 1$, $A = 1$, $B = 0.7$ and $C = 0.1$. It can be seen that all the trajectories are moving away from $\theta = 0$ when $\alpha^* = 0.01$, which indicates instability. In the second case it is stable.

To understand the long term behavior of orbits around the equilibrium positions, a set of orbits with initial positions close to $(\theta, \dot{\theta}) \to (0+, 0+)$ and $(\theta, \dot{\theta}) \to (\frac{\pi}{2}, 0)$ is given in Figures 7 and 8 in the $\theta - \frac{d\theta}{dt}$ phase plane when $\alpha^* = 0.01, k = 1, z_0 = 1, A = 1, B = 0.7$ and $C = 0.1$. These orbits are allowed to evolve for a short period of time and their trajectories are traced in Figure 7. It can

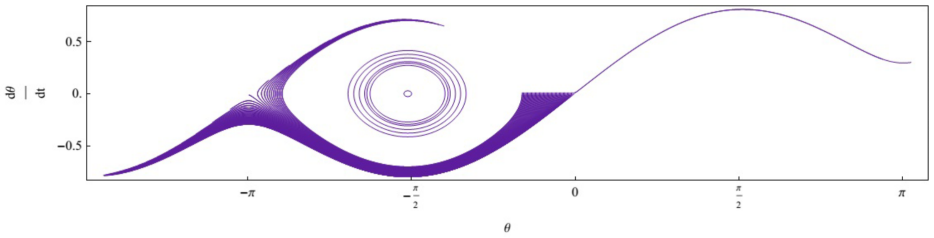

Fig. 9 A set of orbits with initial positions close to $(\theta, \dot{\theta}) \to (0-, 0-)$ in the $\theta - \frac{d\theta}{dt}$ phase plane when $\alpha^* = 0.01, k = 1, z_0 = 1, A = 1, B = 0.7$ and $C = 0.1$.

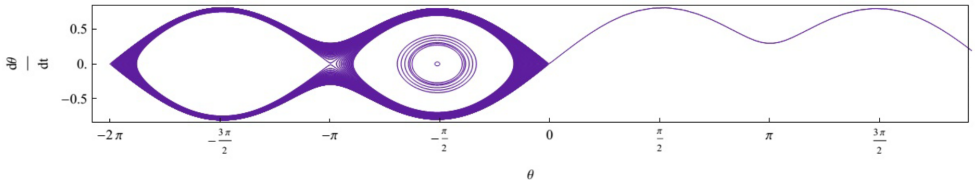

Fig. 10 Same orbits as in Fig. 9 but integrated for a much longer time.

be seen that the orbits starting close to $0+$ (close to 0 and positive) are immediately captured by the nearby stable equilibrium at $\frac{\pi}{2}$. The orbits which start near $(\theta, \dot{\theta}) \to (\frac{\pi}{2}, 0)$ remain in an elliptical orbit around $(\frac{\pi}{2}, 0)$. When these orbits are allowed to evolve for a longer period of time, some of the orbits near $(0+, 0+)$ are captured by the nearby stable equilibrium at $\frac{3\pi}{2}$ and escape after a couple of orbits. The orbits close to $(\frac{\pi}{2}, 0)$ remain in a nearly circular orbit about the center which is strong evidence for the existence of periodic orbits around $(\frac{\pi}{2}, 0)$. A similar analysis is performed for orbits with initial positions close to $(\theta, \dot{\theta}) \to (0-, 0-)$ and $(\theta, \dot{\theta}) \to (-\frac{\pi}{2}, 0)$. It can be seen in Figures 9 and 10 that the orbits starting close to $0-$ (close to 0 and negative) are immediately captured by the nearby center at $-\frac{\pi}{2}$. Some of them, when integrated for a much longer period of time, are captured by the center at $\frac{-3\pi}{2}$. The orbits that start around $(-\frac{\pi}{2}, 0)$ remain in nearly circular orbits around $(-\frac{\pi}{2}, 0)$. Similar behavior is observed around all the spectrally stable equilibriums. Therefore, we can safely conjecture that around each stable equilibrium position there is a family of periodic orbits.

As mentioned earlier and shown in Figures 4 and 5, the number of equilibrium points, when $0 < \theta < 2\pi$, reduces from five to three and in some cases two for higher values of α^* and k. For example, when $B = 0.7, C = 0.1, k = 10, z_0 = 1$ and $\alpha^* = 7$ there are two equilibrium points, $\theta = 2.32$ (stable) and 5.89 (unstable). If $\alpha^* = -7$, i.e. the spacecraft is negatively charged, the positions of the two equilibriums are changed and the stability is reversed. When $|B - C| < 1$, the positions of the equilibrium points are almost identical to what we have shown above. Its effect on stability is explained below.

(1) $\theta = 0, 2\pi$: When $B \geq C$ and $\alpha^* > 0$, the equilibrium positions at $\theta = 0, 2\pi$ will be stable. But when $\alpha^* < 0$, these two equilibrium positions are unstable.
(2) $\theta = \frac{\pi}{2}$: For $B \geq C$ the equilibrium position at $\theta = \frac{\pi}{2}$ is always stable. However, when $B < C$ the value of α^* has to be relatively high in which case $\theta = \frac{\pi}{2}$ will no longer be an equilibrium position.

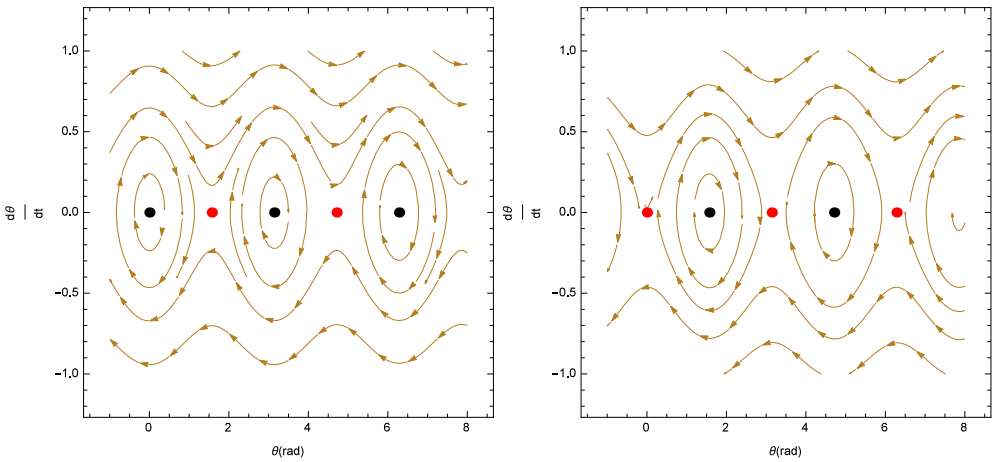

Fig. 11 Trajectory in the $\theta - \frac{d\theta}{dt}$ phase plane when $\alpha = 0.01, k = 1, z_0 = 1$ and (*Left*): $B = 0.5, C = 0.9$. (*Right*): $B = 0.9, C = 0.5$. Black dots correspond to stable equilibrium points and red dots correspond to unstable equilibrium points.

(3) $\theta = \pi$: When $B \leq C$ and $\alpha^* > 0$, $\theta = \pi$ is stable. For a negatively charged spacecraft, $B < C$ is a necessary condition for the stability of the equilibrium position at $\theta = \pi$. Therefore when $B > C$, the value of α^* has to be relatively high in which case $\theta = \pi$ will no longer be an equilibrium position.
(4) $\theta = \frac{3\pi}{2}$: $B > C$ is a necessary and sufficient condition for the stability of the equilibrium position at $\theta = \frac{3\pi}{2}$ unless α^* is very large and negative in which case $\theta = \frac{3\pi}{2}$ will no longer be an equilibrium position.

In summary, when $0 < \alpha^* < 1$ and $B < C$, the equilibrium positions at $\theta = 0, \pi, 2\pi$ are stable and those at $\theta = \frac{\pi}{2}, \frac{3\pi}{2}$ are unstable, and when $B > C$ the nature of the five equilibrium positions is reversed. To demonstrate this behavior, a typical example is given in Figure 11.

3.3 Equations of Motion in the Roll Direction

In this section, we study the attitude motion of the spacecraft in the roll direction, i.e. $\psi = \theta = 0$, $\phi \neq 0$. Applying this condition in the Euler equation for the attitude motion of the spacecraft, we obtain the second order differential equation of the motion in the roll direction.

$$\begin{aligned} C\frac{d^2\phi}{dt^2} &= \Omega^2(A-B)\sin\phi\cos\phi + x_0\sin\phi(kT_{\text{mag}} - R_{\text{mag}}) + x_0\cos\phi(T_{\text{mag}} - kR_{\text{mag}}) \\ &\quad + x_0\sin\phi(kT_{\text{elec}} - R_{\text{elec}}) + x_0\cos\phi(T_{\text{elec}} - kR_{\text{elec}}) + m_1B_2\cos\phi - m_2B_1\sin\phi. \end{aligned}$$

Let $y_0 = kx_0$ then,

$$\begin{aligned} C\frac{d^2\phi}{dt^2} &= \Omega^2(A-B)\sin\phi\cos\phi + x_0\sin\phi(kT_{\text{mag}} - R_{\text{mag}}) + x_0\cos\phi(T_{\text{mag}} - kR_{\text{mag}}) \\ &\quad + x_0\sin\phi(kT_{\text{elec}} - R_{\text{elec}}) + x_0\cos\phi(T_{\text{elec}} - kR_{\text{elec}})\cos\phi + m_1B_2\cos\phi - m_2B_1\sin\phi \\ &= h(\alpha^*, k, \phi, x_0, A, B). \end{aligned} \tag{47}$$

3.4 Derivation of Equilibrium Solutions in the Roll Direction and Their Linear Stability Analysis

In this section, the existence and stability of equilibrium positions in the roll direction of a spacecraft with a general shape under the influence of gravitational torque, Lorentz torque, and geomagnetic torque are discussed. The stability of the equilibrium positions derived is discussed both analytically and numerically. To find the equilibrium positions, set the right hand side of Equation (47) equal to zero which reduces to the following equation for $A = 0.1,\ B = 0.7,\ C = 1,\ x_0 = 1,\ a = 6900\ \text{km},\ i = 51^\circ,\ e = 0.001$ and $f = 60^\circ$.

$$h_1(k,\alpha^*,\phi) = \left[1.036\times10^{-7} + (-0.012 + 9.41k)\alpha^*\right]\times\cos\phi + (-1.13\times10^{-7} + 9.41\times10^{-10}\alpha^* - 0.012k\alpha^*)\sin\phi - 3.63\times10^{-7}\sin(2\phi) = 0. \quad (48)$$

It is not possible to solve equation $h_1(k,\alpha^*,\phi) = 0$ in a closed form as $\phi = f(k,\alpha^*)$; therefore numerical techniques are used to identify all the roots of equation $h_1(k,\alpha^*,\phi) = 0$ which are the desired equilibrium solutions. Let $k = 1$. For $\alpha^* \in (-2.15\times10^{-5}, 2.15\times10^{-5})$, i.e for a very small amount of charge, there are four equilibrium solutions and for higher values of α^* there are two equilibrium solutions.

(1) $\phi_1 \in (0, 0.4)$ when $\alpha^* \in (-2.15\times10^{-5}, 2.15\times10^{-5})$.
(2) $\phi_2 \in (1.47, 1.89)$ when $\alpha^* \in (-2.15\times10^{-5}, 2.15\times10^{-5})$.
(3) $\phi_3 \in (2.80, 3.18)$ when $\alpha^* \in (-2.15\times10^{-5}, 2.15\times10^{-5})$.
(4) $\phi_4 \in (4.37, 4.73)$ when $\alpha^* \in (-2.15\times10^{-5}, 2.15\times10^{-5})$.
(5) $\phi_5 = 2.36$ when $|\alpha^*| > 2.15\times10^{-5}$.
(6) $\phi_6 = 5.5$ when $|\alpha^*| > 2.15\times10^{-5}$.

In the above example $B > A$. Now we switch the values of A and B to have $B < A$ and find the location of the equilibrium positions. In this case, we still have four equilibrium solutions when $\alpha^* \in (-2.15\times10^{-5}, 2.15\times10^{-5})$ and two when $|\alpha^*| > 2.15\times10^{-5}$. All the equilibrium positions when $A = 0.7,\ B = 0.1,\ k = 1,\ C = 1,\ x_0 = 1, a = 6900\ \text{km},\ i = 51^\circ,\ e = 0.001$ and $f = 60^\circ$ are listed below.

(1) $\phi_7 \in (1.23, 1.58)$ when $\alpha^* \in (-2.15\times10^{-5}, 2.15\times10^{-5})$.
(2) $\phi_8 \in (3.12, 3.47)$ when $\alpha^* \in (-2.15\times10^{-5}, 2.15\times10^{-5})$.
(3) $\phi_9 \in (4.69, 5.04)$ when $\alpha^* \in (-2.15\times10^{-5}, 2.15\times10^{-5})$.
(4) $\phi_{10} \in (5.97, 6.32)$ when $\alpha^* \in (-2.15\times10^{-5}, 2.15\times10^{-5})$.
(5) $\phi_{11} = 2.36$ when $|\alpha^*| > 2.15\times10^{-5}$.
(6) $\phi_{12} = 5.5$ when $|\alpha^*| > 2.15\times10^{-5}$.

As $y_0 = kx_0$ we can take $x_0 = 1$. To reduce the dimensions, without loss of generality, we define $ab = A - B$ and rewrite $h_1(k,\alpha^*,\phi,ab)$ as below.

$$h_1(k,\alpha^*,\phi,ab) = \left[-1.13\times10^{-7} + 10^{-3}(6k-15)\alpha^*\right]\cos\phi + (1.03\times10^{-7} + 10^{-3}(6-15k)\alpha^*)\sin\phi + 6.05\times10^{-7}ab\sin(2\phi).$$

It can be seen from Figure 12 that there are four equilibrium solutions for small values of α^* and all values of ab when $k = 1$. For higher values of α^* there are only two equilibrium solutions at $\phi = 2.3$ and $\phi = 5.5$ for all values of ab. We have seen above that for $k = 1$, the changing values of ab and α^* have a significant effect on the existence of equilibrium solutions in the roll direction. To see this for $k \neq 1$, we plot $h_1(k,\alpha^*,\phi,ab) = 0$ for fixed values of $ab = 0.3$, and $ab = -0.3$ in Figure 13. It is clear from Figure 13 that with the changing value of k, the position of equilibrium changes significantly but the number of equilibrium positions remains four as before both for negative and

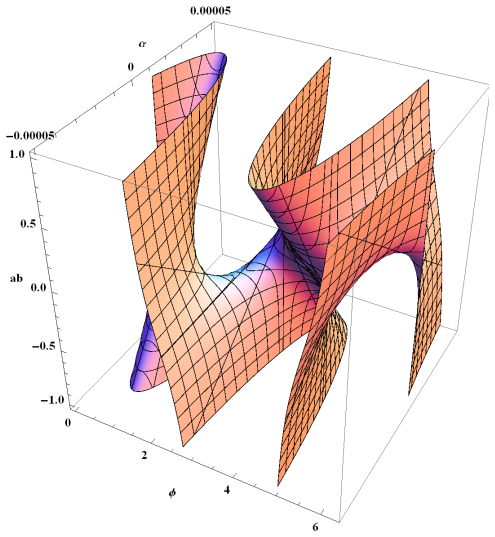

Fig. 12 Implicit plot of $h(\alpha, \phi, ab) = 0$.

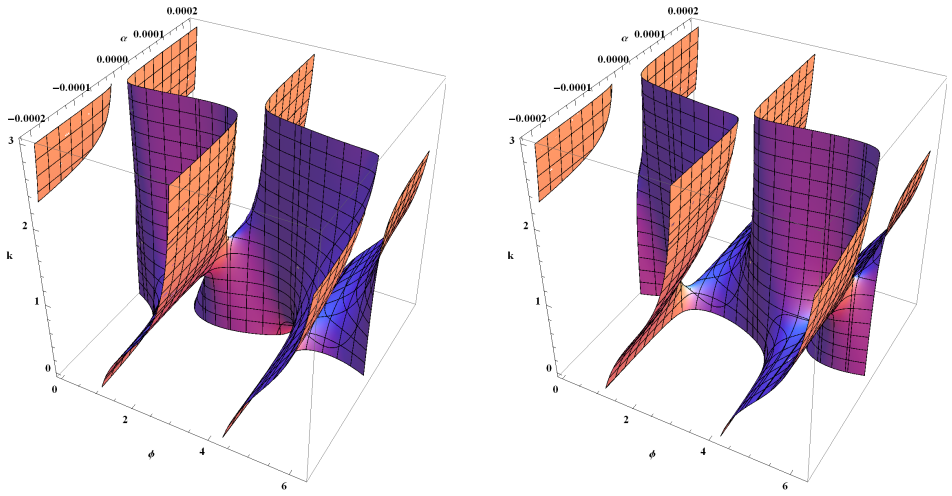

Fig. 13 Implicit plots of $h(\alpha, \phi, k, ab) = 0$ when (*left*) $ab = -0.3$ and (*right*) $ab = 0.3$.

positive values of ab when α^* is small. The effect of ab is significant when $k < 1$. For higher values of α^*, the number of equilibrium positions remains two but their positions change with the changing values of ab and k, see Figures 12 and 13.

To study the stability of the derived equilibrium position, we use the same method that was used for the pitch direction. We write Equation (47) as a system of two first order equations, linearize them and find the eigenvalues of the Jacobian matrix from the equation given below.

$$\lambda^2 - h_\phi(\alpha^*, k, \phi, ab) = 0\,. \tag{49}$$

It can be seen from Equation (49) that there are only two types of eigenvalues possible. If $h_\phi(\alpha^*, k, \phi, ab) > 0$ there exist two eigenvalues: one of which is negative and the other is positive.

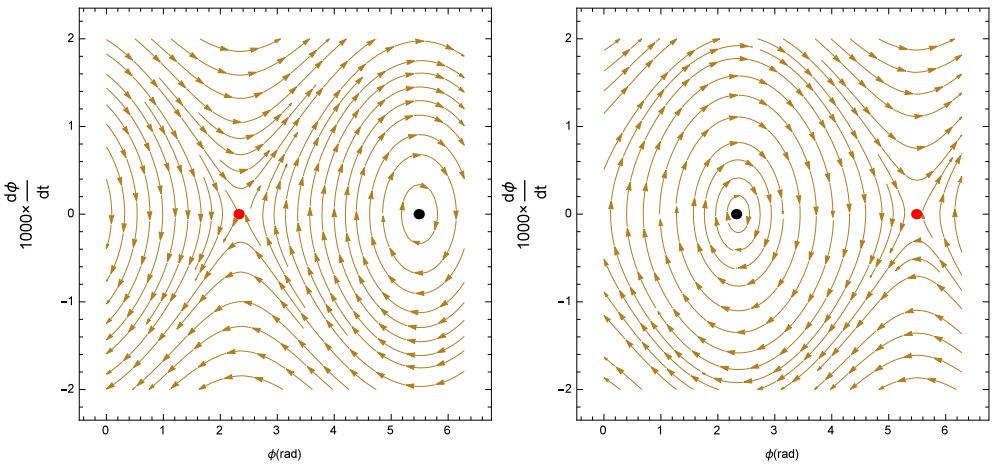

Fig. 14 Trajectory in the $\phi - \frac{d\phi}{dt}$ phase plane when (*left*) $\alpha^* = 0.1, k = 1, z_0 = 1$ and $ab = -0.6$, (*right*) $\alpha^* = -0.1, k = 1, z_0 = 1$ and $ab = -0.6$.

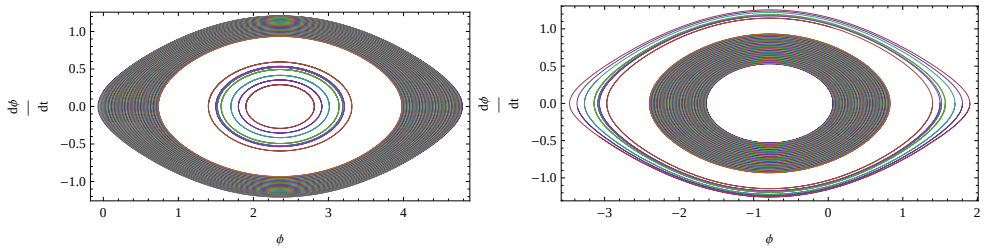

Fig. 15 A set of orbits with initial positions close to the equilibrium positions when $e = 0.1, ab = 0.6$ and (*left*) $\alpha^* = -0.1$, (*right*) $\alpha^* = 0.1$.

Therefore, $h_\phi(\alpha^*, k, \phi, ab) > 0$ becomes a sufficient condition for instability. If $h_\phi(\alpha^*, k, \phi, ab) < 0$ the equilibrium point in question will be spectrally stable or a stable center. We will investigate the equilibrium points obtained above for $ab = 0.6,\ ab = -0.6,\ k = 1,\ x_0 = 1, a = 6900\,\text{km},\ i = 51^\circ,\ e = 0.001$ and $f = 60^\circ$, and write $h_\phi(\alpha^*, \phi, ab)$ as below.

$$\begin{aligned} h_\phi(\alpha^*, \phi)|_{ab=-0.6} \ = \ & (-1.13 \times 10^{-7} - 0.01\alpha^*)\cos\phi - 7.26 \times 10^{-7}(\cos\phi)^2 \\ & +(-1.04 \times 10^{-7} + 0.01\alpha^* + 7.26 \times 10^{-7}\sin\phi)\sin\phi\,. \end{aligned}$$

The equilibrium positions at ϕ_1 and ϕ_3 are stable, as in these cases $h_\phi(\alpha^*, \phi)|_{ab=-0.6} < 0$. Similarly, ϕ_2 and ϕ_4 are unstable, as in these cases $h_\phi(\alpha^*, \phi)|_{ab=-0.6} > 0$. By similar arguments, ϕ_5 will be an unstable equilibrium if the spacecraft is positively charged and ϕ_6 will be unstable if the spacecraft is negatively charged. Likewise, when $ab = 0.6$, ϕ_7 and ϕ_9 are stable, ϕ_8 and ϕ_{10} are unstable, ϕ_{11} is stable when $\alpha^* < -1.11 \times 10^{-6}$ and ϕ_{12} is stable when $\alpha^* > 3.25 \times 10^{-7}$. A typical example is given in Figure 14 when $ab = \pm 0.6$. The equilibrium at $\phi = 2.36$ is stable when $\alpha^* = -0.1$ and unstable when $\alpha^* = 0.1$. Similarly, the equilibrium at $\phi = 5.5$ is unstable when $\alpha^* = -0.1$ and stable when $\alpha^* = 0.1$.

To understand the long term behavior of orbits around the equilibrium positions, a set of orbits with initial positions close to the equilibrium are given in Figures 15 and 16 in the $\phi - \frac{d\phi}{dt}$ phase

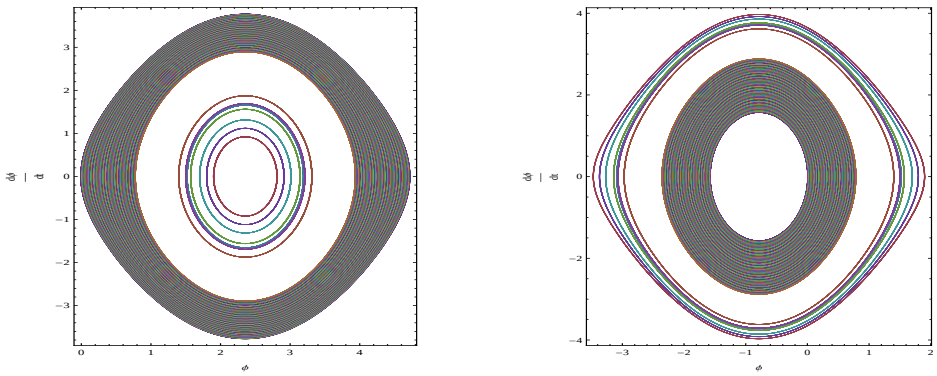

Fig. 16 A set of orbits with initial positions close to the equilibrium positions when $e = 0.1, ab = 0.6$ and (*left*) $\alpha^* = -1$, (*right*) $\alpha^* = 1$.

plane when $\alpha^* = \pm 0.1, \pm 1$, and $k = 1, z_0 = 1, ab = 0.6, e = 0.1$. These orbits are allowed to evolve for a long period of time and their trajectories are traced in Figures 15 and 16. The orbits in Figure 15 (left) are given for $\alpha^* = -0.1$ and it can be seen that all the orbits are captured by the equilibrium position at $\phi = 2.36$, which is a stable equilibrium. The orbits that are closer to the stable equilibrium position remain in a perfect periodic orbit while the orbits that are not so close have an elliptical orbit in the vicinity of the equilibrium position but are not necessarily periodic. For $\alpha^* = 0.1$ in Figure 15 (right), the equilibrium position at $\phi = 2.36$ is unstable. Hence the same orbits are captured by another nearby stable equilibrium at $\phi = -0.723$ which is a mirror image of the stable equilibrium at $\phi = 5.56$. When the same orbits are integrated for $\alpha^* = \pm 1$, similar behavior is observed. Also, similar behavior is observed around all the stable equilibriums. Therefore, we can safely conjecture that around each stable equilibrium position there is a family of periodic orbits.

4 CONCLUSIONS

This paper discussed the attitude stabilization of a charged spacecraft moving in an elliptical orbit using Lorentz torque. The Lorentz torque is developed in two parts, T_{mag} and T_{elec}. T_{mag} is the Lorentz torque that is experienced by a magnetic field and T_{elec} is the Lorentz torque experienced by an electric dipole moment in the presence of an electric field. The model we developed incorporates all Lorentz torques as a function of orbital elements and the radius vector of the charged center of the spacecraft relative to its center of mass. We investigated, both analytically and numerically, the existence and stability of equilibrium positions in both pitch and roll directions. In the pitch direction, there are a total of five equilibrium points at $\theta = n\pi/2, n = 0, 1, 2, 3, 4$ when $-1 < \alpha^* = q/m < 1$, $0 < k < 1$ and $\theta \in [0, 2\pi]$. Their stability is analyzed for changing values of the charge to mass ratio, α^*, and it is shown that α^* affects the stability and existence of equilibrium positions. The equilibrium positions at $\theta = 0, 2\pi$ are unstable for $\alpha^* > 0$ when $B = 0.7$ and $C = 0.1$. These two equilibrium positions are stable when $B = 0.1$ and $C = 0.7$. These equilibrium positions are also stable for $\alpha^* < 0$.

We have shown that the sign and amount of charge play a significant role in determining the equilibrium positions and their stability. In the case of the roll direction, we have four equilibrium points when $\alpha^* \in (-2.15 \times 10^{-5}, 2.15 \times 10^{-5})$ and only two equilibrium positions when $\alpha^* \notin (-2.15 \times 10^{-5}, 2.15 \times 10^{-5})$. It is demonstrated both analytically and numerically that almost all the equilibrium positions depend on the values and sign of charge to mass ratio both in terms of existence and stability. In the same way as in the pitch direction, the equilibrium positions that are

stable for $A < B$ become unstable when $A > B$ and vice versa. This is not true in general but this happens in most of the cases. Here A, B and C refer to the components of moment of inertia of the spacecraft.

References

Abdel-Aziz, Y. 2007a, Applied Mathematical Sciences, 1, 1511
Abdel-Aziz, Y. A. 2007b, Advances in Space Research, 40, 18
Abdel-Aziz, Y. A., & Khalil, K. I. 2014, RAA (Research in Astronomy and Astrophysics), 14, 589
Abdel-Aziz, Y. A., & Shoaib, M. 2014, RAA (Research in Astronomy and Astrophysics), 14, 891
Gangestad, J. W., Pollock, G. E., & Longuski, J. M. 2010, Celestial Mechanics and Dynamical Astronomy, 108, 125
Heilmann, A., Ferreira, L. D. D., & Dartora, C. A. 2012, Brazilian Journal of Physics, 42, 55
Hiroshi, Y. Katsuyuki, Y., & Mai, B. 2009, Twenty-seventh International Symposium on Space Technology and Science (*http://www.ists.or.jp/2009/*)
Peck, M. A. 2005, in AIAA Guidance, Navigation and Control Conference, San Francisco, CA, AIAA 2005–5995
Peng, C., & Gao, Y. 2012, Acta Astronautica, 77, 12
Pollock, G. E., Gangestad, J. W., & Longuski, J. M. 2011, Acta Astronautica, 68, 204
Streetman, B., & Peck, M. A. 2007, Journal of Guidance Control Dynamics, 30, 1677
Tikhonov, A. A., Spasic, D., Antipov, K. A., & Sablina, M. 2011, Automation and Remote Control, 72, 1898
Ulaby, F. T. 2005, Electromagnetics for Engineers (Pearson/Prentice Hall)
Vokrouhlicky, D. 1989, Celestial Mechanics and Dynamical Astronomy, 46, 85
Wertz, J. R. e. a. 1978, Spacecraft Attitude Determination and Control (D. Reidel Publishing Company, Dordecht, Holland)
Yamakawa, H., Hachiyama, S., & Bando, M. 2012, Acta Astronautica, 70, 77